RSC Advances

PAPER

View Article Online
View Journal | View Issue

Cite this: *RSC Adv.*, 2022, **12**, 7328

Preparation and MRI performance of a composite contrast agent based on palygorskite pores and channels binding effect to prolong the residence time of water molecules on gadolinium ions†

Minzhi Zhao,[a] Zhonghua Tang,[b] Jia Zhang,[a] Guorui Fu,[a] Weibing Xu,[a]* Qingfeng Wu[c] and Lumei Pu*[a]

Received 10th December 2021
Accepted 26th February 2022

DOI: 10.1039/d1ra08967f

rsc.li/rsc-advances

Herein, gadolinium tannate was simply and conveniently coated on the surface of palygorskite by *in situ* reaction of a coordination polymer formed between tannic acid and Gd^{3+}. The palygorskite–tannate gadolinium–polyvinyl alcohol integrated composite (PAL@Gd@PVA) is successfully prepared after the introduction of polyvinyl alcohol onto the palygorskite–tannate gadolinium. The structure is characterized by Fourier transform infrared spectroscopy, thermogravimetric analysis, X-ray diffraction spectroscopy, X-ray photoelectron spectroscopy, and transmission electron microscopy analysis. The results show that TA-Gd and PVA are successfully loaded on the surface of palygorskite, and the rod crystal structure of palygorskite in the composite remains intact. Palygorskite fibres constitute the framework of the composite and play a key role in supporting and crosslinking the composite. The prepared compounds showed negligible cytotoxicity and low haemolysis rate, showing good biocompatibility. *In vitro* MRI results showed that the longitudinal and transverse relaxation rates of the composite are 59.56 and 340.81 mm^{-1} s^{-1}, respectively.

Introduction

Magnetic resonance imaging (MRI) is an imaging method based on the difference of relaxivity time between different tissues of the human body. It has attracted more and more attention for its advantages of high spatial resolution, having no limitation of tissue penetration ability and its harmlessness for the human body.[1–4] However, many organs and tissues in the human body are similar in density and relaxivity rate and other characteristics. In order to increase the contrast of images of different tissues and improve the accuracy of diagnostic results, a contrast agent needs to be injected before MRI testing.[5,6] MRI contrast agents can be divided into two types, namely T1 and T2. T1 contrast agents enhance MRI signals by reducing the longitudinal relaxation time of protons in water molecules around tissues, and are also known as positive contrast agents because of their role in increasing brightness of MRI images. T2 contrast agents weaken the magnetic resonance imaging signal by reducing the transverse relaxation time of protons in water molecules around tissues, and are also known as negative contrast agents because of their effect on increasing the darkness of MRI images.[7–9] It is mainly 1 contrast agents that enhance the signal that have been approved for clinical use. Among them, the gadolinium (Gd) ion has seven unpaired electrons outside the nucleus, which exhibits the strongest paramagnetism and can enhance MRI signal intensity to the greatest extent and is widely used as a T1 type contrast agent.[10] However, the commercially used Gd-based MRI CAs suffer low relaxivities and insufficient stability.[11] The development of MRI CAs with high relaxivity and high stability is of essential importance in both academic and clinical applications. Based on the Solomon–Bloembergen–Morgen (SBM) theory,[12] the relaxivity can be significantly enhanced by tuning three important parameters: (i) the number of inner-sphere water molecules directly coordinated to the Gd(III) centre, q; (ii) the residence time of the coordinated water molecule, τ_M; (iii) rotational correlation time representing the molecular tumbling time of a complex, τ_R.[13] A widely used strategy is appending Gd(III) complexes to a macromolecular platform,[14] such as dendrimers,[15] proteins,[16] and other kinds of slow rotating objects,[17,18] to prolong τ_R for the enhancement of relaxivity. However, this method only uses the property of slow rotation velocity of carrier to extend τ_R, and the improvement of relaxation rate by this method is limited. If the water molecules near gadolinium ion can be bound simultaneously to reduce the water exchange rate, the relaxation rate can be further improved.

[a]College of Science, Gansu Agricultural University, Lanzhou 730000, China. E-mail: xuwb@gsau.edu.cn
[b]Lanzhou Petrochemical Research Centre, PetroChina, Lanzhou 730060, Gansu, China
[c]Institute of Modern Physics, Chinese Academy of Sciences, Lanzhou 730000, China

† Electronic supplementary information (ESI) available: The XPS spectra, erythrocyte haemolysis, and cellular viability. See DOI: 10.1039/d1ra08967f

Palygorskite (PAL) is a natural nanometer rod-like hydrated magnesium aluminum silicate mineral and the theoretical formula of $Mg_5Si_8O_{20}(OH)_2(H_2O)_4 \cdot nH_2O$, which consisting of two double chains of the pyroxene-type $(SiO_3)^{2-}$ like amphibole $(Si_4O_{11})^-$ running parallel to the fibre axis.[19] PAL is rich in pores and channels due to its unique crystal structure and stacking pattern, including micropores and mesopores within the crystal texture, as well as macropores between particles.[20] A variety of water molecules are bound in the abundance of pores and channels of PAL. These bound water molecules are stable and cannot be completely volatilized even when heated.[21] When these water molecules, which have lost their freedom due to the restriction of pores and channels of PAL, contact with gadolinium ions, the residence time on gadolinium ions will be greatly extended, thus greatly improving the relaxivity properties of contrast agents. Inspired by the effect of pore bound water molecules, herein, gadolinium ion is introduced into the outlet of the surface pores and channels of PAL by the technique of *in situ* forming a coordination polymer layer on the surface of PAL with metal gadolinium ion and tannic acid. The results showed that gadolinium ions were successfully introduced into the surface of PAL and the rod crystals of PAL remained intact. The designed and prepared composites show good biocompatibility and negligible cytotoxicity. Moreover, as MRI contrast agent, the longitudinal relaxation rate *in vitro* of the composite is up to 59.56 mm^{-1} s^{-1}, shows a good application prospect.

Experiment

Materials and characterize

Palygorskite (PAL) was purchased from Jiangsu Palygorskite International Co., Ltd. Gadolinium chloride hexahydrate ($GdCl_3 \cdot 6H_2O$, 99%) was purchased from Shanghai Yuanye Biotechnology Co., Ltd. Polyvinyl alcohol (PVA) was purchased from Shanghai Aladdin Biochemical Technology Co., Ltd. DMEM medium, 3-(4,5-dimethylthiazole-2-yl)-2,5-dipheny-ltetrazolium bromide (MTT) and Fetal bovine serum (FBS) were purchased from Beijing Solar bio Science & Technology Co., Ltd. Dimethyl sulfoxide (DMSO) and tannic acid (TA) were purchased from Tianjin Hengxing Chemical Reagent Manufacturing Co., Ltd. Kunming mice were purchased from Lanzhou University Medical College. Deionized water (H_2O) laboratory homemade.

Preparation of PAL@Gd-*n*

500 mg PAL were accurately weighed and dispersed in 4.5 ml deionized water. Then it was crushed by ultrasound in ice bath for 10 min to obtain 10% PAL solution. 0.5 ml and 1.0 ml 10% PAL solutions were added to 4.4 ml and 3.9 ml deionized water, respectively. Then 50 μL tannic acid solution (40 mg ml^{-1}) was added to all the above solutions, and vortexed for 3 min. Then add 50 μL $GdCl_3 \cdot 6H_2O$ solution (10 mg ml^{-1}) and vortex for 5 min. Finally, 5 ml MOPS solution was added to the solutions and vortexed for 5 min. Then centrifuged them at 8000 rpm for 10 min and washed with distilled water for three times. Then remove the supernatant, and dispersed in 5 ml distilled water to obtain PAL@Gd-*n*, *n* was 0.5 and 1.0.

Preparation of PAL@Gd-*n*@PVA

0.5 g PVA and 20 ml distilled water were added to a round-bottomed flask. Then put it in an oil bath stir to dissolve at 50 °C. 1.0 ml PVA solution was added to the PAL@Gd-*n* solution. The solution was stirred overnight at room temperature, then, centrifuged at 8000 rpm for 10 min, washed with distilled water for three times. Then remove the supernatant, and the solid obtained was PAL@Gd-*n*@PVA.

Characterization

Fourier transform spectra were measured on an iS50 FT-IR(Nicolet) spectrophotometer. Samples were thermogravimetric analysed with Netzsch STA 409 PC Analyzer at a heating rate of 10 °C min^{-1} from 25 °C to 900 °C. The particle size and zeta potential of PAL-TA-Gd were measured by zeta particle size analyser (SALD, 2300, SHIMADZU, Japan) at room temperature. XPS analysis was performed on the samples using VG Multi-Lab 2000. XRD data of PAL and PAL@Gd-*n*@PVA were measured at XRD-6100(Shimadzu, Japan). TEM images were acquired by JEM-2100 (Japan Corporation) at 200 kV. Enzyme marker (RT-6100) Shenzhen Leidu Life Technology Co., Ltd. The dissociation amount of Gd^{3+} in the matrix was measured by ICPPLASMA 1000. The T1 and T2 weighted images and *in vivo* imaging of the samples were collected on the 1.0 T nuclear magnetic resonance analyser (Ningbo Chuanshanjia Electrical and Mechanical Co., Ltd., China).

Cell cytotoxicity assay

PAL@Gd-0.5@PVA was selected as the representative to test the following performance. Human umbilical vein endothelial cells (HUVEC) were cultured in DMEM medium. 10% fetal bovine serum (FBS), 100 U mL^{-1} penicillin and 0.1 mg ml^{-1} streptomycin were added to each medium. The cells were stored in an incubator with 5% CO_2, 37 °C. The cytotoxicity of PAL@Gd-0.5@PVA was evaluated with HUVEC cells by MTT assay. Typically, 100 μL HUVEC cells (0.5–5 × 10^3/well) cultured with DMEM were inserted into a 96-well plate and cultured overnight for adherent growth. Then add different concentrations of (25, 50, 100, 200, 400 μg L^{-1}) PAL@Gd-0.5@PVA solutions for 48 h, add 20 μL MTT (5 mg ml^{-1}) to each well, incubate in an incubator. After 4 h, the 96-well plate was taken out and 150 μL DMSO was added to each well. Then shock for 10 min. The absorbance (OD) was recorded under a 490 nm microplate to evaluate the cytotoxicity.

Hemolytic test

Taking seven centrifuge tubes, add 400 μL 2% red blood cell suspension to each tube, then add 400 μL PAL@Gd-0.5@PVA solution of different concentrations (25 μg L^{-1}, 50 μg L^{-1}, 100 μg L^{-1}, 200 μg L^{-1} and 400 μg L^{-1}) to five of them, respectively. The other two tubes were filled with equal volume (400 μL) of distilled water and PBS buffer as positive control and negative control, respectively. All the centrifuge tubes were placed in an incubator at 37 °C for 1 h, then centrifuged at 3000 rpm for 10 min. Finally, 100 μL supernatant was transferred to the 96-

well plate, and the OD value of each well on the 96-well plate was measured with a microplate analyser at 540 nm.

In vitro and *vivo* MRI test

PAL@Gd-0.5@PVA was selected as the representative to test MRI performance. The sample was dispersed in deionized water and the concentration was set to be 0.009–0.03 mmol L^{-1} (equal Gd^{3+} concentrations). The longitudinal relaxation time (T1) and transverse relaxation time (T2) were measured by 1.0 T MRI scanner. T1 was measured using a standard reverse recovery pulse series. T2 measurements were made using the CPMG spin echo magnetic pulse series. Then, according to the graph of $T1^{-1}$, $T2^{-1}$ *vs.* Gd^{3+}, the relaxation rate of r1 and r2 were calculated.

The 8 week-old Kunming mice were injected with 60 μL 8% chloral hydrate to induce anesthesia (Experimental Animal Centre of Lanzhou University, 20 ± 2 g). Then 300 μL PAL@Gd-0.5@PVA solution was injected through the tail vein ($n = 3$), and scanning imaging was performed on the mice for 1 h, 2 h, 4 h, 6 h and 8 h, respectively. The control group received PBS. Finally, a scan was performed 24 h after injection. The T1-weighted imaging parameters were set as follows: TR/TE = 360/11 ms; matrix = 256 × 256; slice thickness = 0.3 mm; 128 slices and inter slice gap = 0.3 mm. All animal procedures and euthanasia were performed in accordance with the Guidelines for Care and Use of Laboratory Animals of Gansu agricultural University and approved by the Animal Ethical and Welfare Committee of Gansu agricultural University.

Results and discussion

Preparation and characterization

The design and preparation process based on PAL contrast agent is shown in Scheme 1. Firstly, a coordination polymer layer formed by tannic acid and gadolinium ions is coated on the surface of PAL in a weakly alkaline aqueous solution, and gadolinium ions are introduced into the outlet of the pores and channels on the surface of PAL, so as to block the water molecules in the pores and channels. It is named as PAL@Gd-*n*, *n* represents the added amount of PAL. Then, a long chain of polyvinyl alcohol is introduced to wrap the PAL@Gd-*n*, which improved the stability and biocompatibility of the PAL@Gd-*n* and formed the final composite material PAL@Gd-*n*@PVA. Firstly, the PAL, TA and two composites are studied by FTIR and the result is showed in Fig. 1a. As for the PAL, the characteristic absorption peak at 3600 cm^{-1} belongs to the stretching vibration of Si–OH,[22,23] while the absorption peak at 976 cm^{-1} corresponds to the stretching vibration of Si–O–Mg.[24,25] In the IR spectrum of TA, the absorption peaks at 3300 cm^{-1} belong to the stretching vibration of –OH, while the absorption peaks at 1190 cm^{-1} and 1606 cm^{-1} belong to the asymmetric stretching vibration of C–O and C=C,[26] respectively. By comparison, it can be found that the vibration peak of the both composites at 3600 cm^{-1} is corresponded to the stretching vibration of Si–O in PAL, while the stretching and bending vibration of the aromatic ring carbonyl and C–O and C–C in the TA of the both composites are in the wavenumber range of 1150–1750 cm^{-1}, respectively. Similarly, the characteristic vibration peaks of C–O and C–C in the structure of PVA are covered in the above regions due to the lack of characteristic vibration functional groups. In addition, the characteristic absorption peaks at 976 cm^{-1} of PAL and 1190 cm^{-1} of TA appeared in the both composites, indicating that TA and Gd^{3+} are successfully coated on the surface of PAL. Meanwhile, it can be found that the absorption peak intensity at 976 cm^{-1} in PAL@Gd-1.0@PVA is larger, which may be caused by more APT content in the composite. Fig. 1b shows the TGA curves for PAL and the both composites. It can be seen from the curve of PAL that the mass loss is about 7% when the temperature increases from 25 to 150 °C, which is caused by the loss of water adsorbed on the surface of PAL, and the subsequent weight loss of about 700 °C can be attributed to the loss of water of crystal in PAL.[27] The total weight loss of 17.03% is observed after calcination at 800 °C. During the calcination process of the both composites, the loss of weight is about 8% at 100 °C, which is related to the volatilization of surface adsorption water. The next loss may be related to oxidative condensation and carbonization of TA and PVA at about 300 °C.[28] The

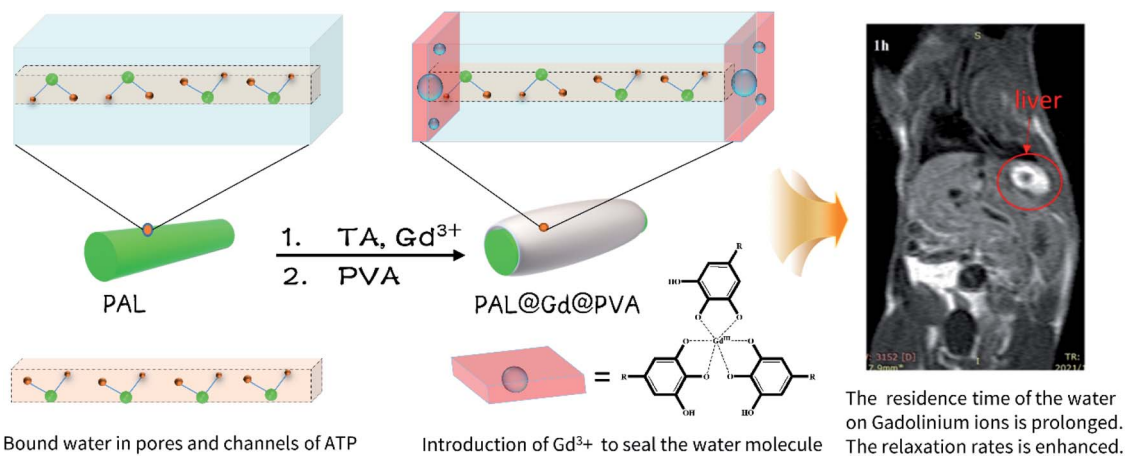

Scheme 1 The fabrication process of the PAL@Gd@PVA composite MRI contrast agent.

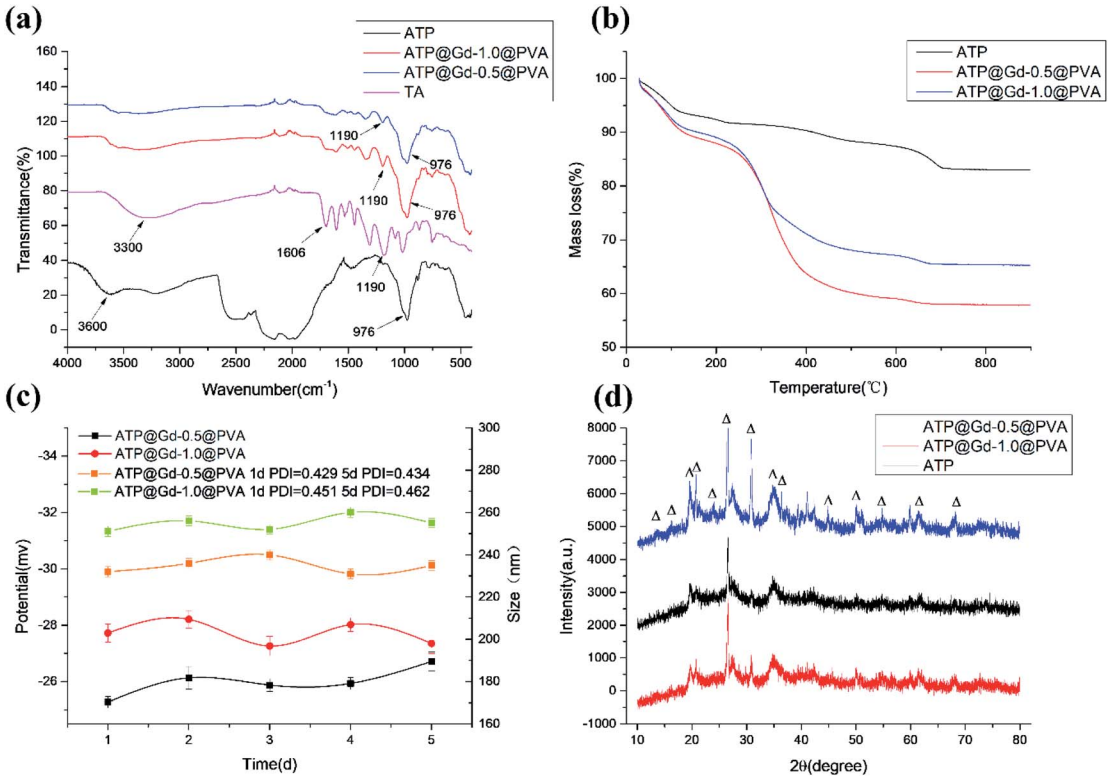

Fig. 1 (a) FTIR spectra, (b) TGA curves, (c) size and zeta potential, (d) XRD pattern of the PAL, PAL@Gd-*n*@PVA composites.

last slow weight loss can be attributed to the complete combustion degradation of TA and PVA after carbonization at 600 °C.[29] The total weight loss of both composites is 42.16% and 34.72%, respectively. The weightlessness of both composites is greater than that of free APT, which is due to the introduction of high temperature-degradable TA and PVA in the both composites, indicating that the coordination polymer formed by TA and Gd^{3+} is successfully loaded on PAL. In additional, However, the weight loss ratio of PAL@Gd-0.5@PVA is greater than that of PAL@Gd-1.0@PVA, which may be related to the PAL content in PAL@Gd-1.0@PVA being higher than that in PAL@Gd-0.5@PVA. The stability of the both composites is assessed by particle size and potential changes over time. The results are shown in Fig. 1c. It can be seen that the particle sizes of the prepared compounds PAL@Gd-0.5@PVA and PAL@Gd-1.0 @PVA are about 230 nm and 250 nm at the first day, and the PDI are 0.429 and 0.451, respectively. With the extension of time to the fifth day, the corresponding particle sizes are 232 and 247 nm, and the PDI increases to be 0.434 and 0.462, respectively. Similarly, the zeta potential of the both composites are −25.27 and −27.72 mV respectively on the first day, which also show insignificantly change with the extension of standing time, showing good stability. Meanwhile, the larger negative potential of the composite material is conducive to the circulation and biological activity of the material *in vivo*.[30] Fig. 1d shows the XRD patterns of PAL and the both composites. It can be seen that there are obvious diffraction peaks at diffraction angles 2θ = 14.12, 17.03, 19.9, 20.8 and 27.7°, which corresponding to the (200), (130), (040), (121) and (400) crystal plane of PAL,[31] respectively. After the composite was formed, the positions of diffraction peaks in the both composites are not significantly different from those of free PAL, indicating that the rod structure of PAL is not damaged in the preparation process of the composite, and the rod structure of PAL played a good role in the skeleton support of the composites. However, the intensity of each diffraction peak decreases significantly in both composites, indicating that the crystallization performance of PAL decreases after the composite is formed, which may be caused by the introduction of TA-Gd coordination polymer coating on the surface.[32]

The surface element composition of the composite is tested by selecting PAL@Gd-0.5 @PVA as the representative. Fig. S1a† shows the XPS survey spectrum of the composite. In addition to Si, Mg and Al elements in PAL,[33] the peaks with binding energies at 284, 531 and 1218 eV can be found, which corresponding to C 1s, O 1s and Gd 3d, respectively. The presence of C, O and Gd on the sample surface indicates that TA–Gd coordination polymer layer is successfully loaded on the surface of PAL. Fig. S1b† is deconvoluted C 1s XPS spectra. Fitting results show that C 1s is divided into three forms, corresponding to C–C, C=C and C–O respectively,[34] which are derived from TA and PVA. The high-resolution O 1s spectrum (Fig. S1c†) can be fitted into three bonding structures, corresponding to O–C, O–C, and O–Gd.[35] In order to confirm that Gd^{3+} is successfully coated on the PAL, high resolution XPS spectra of Gd 4d is summarized in Fig. S1d.† Two strong binding peaks with the binding energy of 142.8 eV and 153.6 eV can be detected, which correspond to the Gd $3d_{5/2}$ and Gd $3d_{3/2}$ energy level.[3] The microscopic

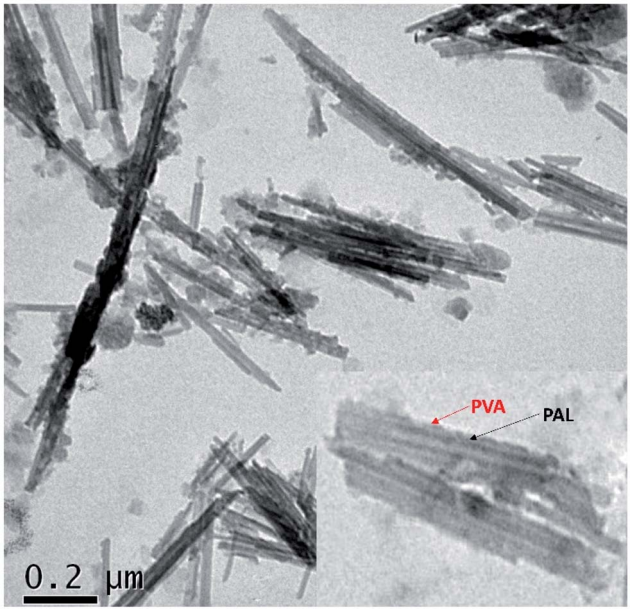

Fig. 2 TEM images of PAL@Gd-0.5@PVA composite.

morphology and structure of PAL@Gd-0.5@PVA are analysed by TEM (Fig. 2). Low-resolution TEM showed that the rods of APT is uniformly dispersed in the composite, with rod crystal length of about 200 nm and diameter of about 30 nm. There is no obvious agglomeration of PAL in the composite. However, it is obvious that after the coating of TA–Gd coordination polymer, the surface of PAL becomes rough and uneven, and some of the surface is sporadically embedded with granular materials from the high-resolution images (the inserted local magnified TEM), which may be assigned to the TA–Gd coordination polymer and PVA successfully coated on the surface of PAL.

In vitro activity research

Good blood compatibility is the prerequisite for the application of bioactive materials. Haemolytic test is often used to evaluate the blood compatibility of materials. The results before and after co-incubation of different concentrations of PAL@Gd-0.5@PVA with freshly collected chicken blood are shown in Fig. S2.† Deionized water and PBS are selected as the positive and negative controls, and it could be seen that only the positive controls had obvious rupture of RBC after incubation and centrifugation, while the others all had good hemolysis. The hemolysis of the composite PAL@Gd-0.5@PVA is 1.46%, 1.62%, 2.11%, 3.41% and 3.88%, respectively (Fig. S3a†), with the concentration increases from 25 to 400 μg ml^{-1}. Which further indicates that the composite material had no obvious damage to red blood cells and had good blood compatibility.[36] In view of the high Gd content in PAL@Gd-0.5@PVA, it is selected as a representative to test the *in vitro* activity of the composite. The content of Gd^{3+} in PAL@Gd-0.5@PVA composite is accurately measured by ICP-MS and 5% nitric acid solution is used as the solvent.[37] The standard curve and test results are shown in Fig. S3b.† It can be seen that the R^2 value of the standard curve is 0.99936, showing a good linear correlation. The Gd^{3+} concentration in PAL@Gd-0.5@PVA solution is also tested for ICP-MS and the absorption strength is compared to the standard curve to obtain accurately the concentration of Gd^{3+} in the solution at 82.2 mg L^{-1}. HUVEC cells are selected as the model, and the cytotoxicity of the prepared composite is studied using MTT method, the results show in Fig. S3c.† It can be seen that the survival rate of HUVEC cells is as high as 96.4% at low concentrations, which basically as same as that of the control group. Cell activity is as high as 95% even at concentrations of up to 400 μg L^{-1}. It is shown that the prepared composite has no obvious toxic effect on HUVEC cells, shows good biocompatibility, and can be used as a contrast agent.

On the basis of the above study, the *in vitro* MRI performance of PAL@Gd-0.5@PVA composite solution is tested. Fig. 3a is a T1, T2 weighted image of different Gd^{3+} concentration solutions (25, 50, 100, 200 and 400 μg L^{-1}), and deionized water as a control. It can be seen that the T1 and T2-weighted images gradually become brighter with the increase of Gd^{3+} concentration, but the brightness of T1 image is higher than that of T2 image, which further indicates that the composite can be used as a T1 contrast agent.[28] Then the longitudinal (T1) and transverse (T2) relaxation times of the solution are tested respectively, and the reciprocal of T1 and T2 are plotted against the Gd^{3+} concentration, and linear fitting is performed. Then the slope of the fitted curve corresponds to the longitudinal (r1) and transverse (r2) relaxivity rate, the result is shown in Fig. 3b. The longitudinal (r1) and transverse (r2) relaxation rates of the

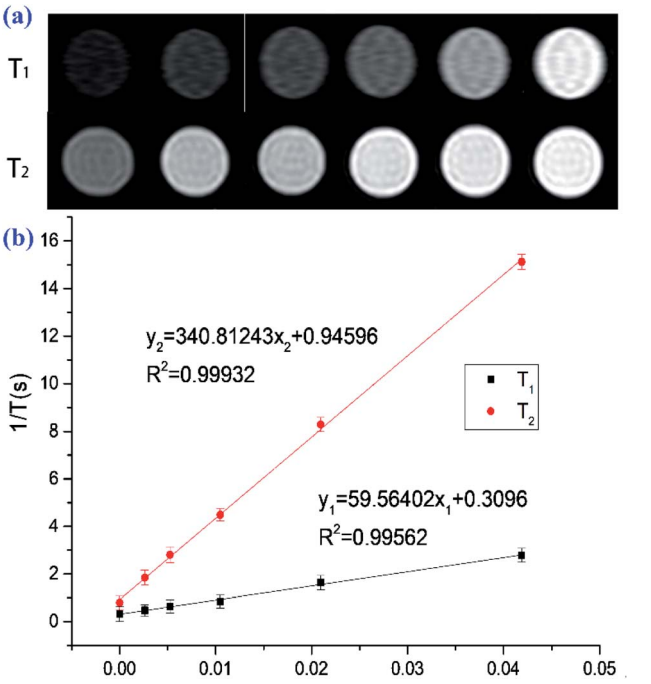

Fig. 3 (a) T1/T2-weighted MR images of PAL@Gd-0.5@PVA composite to pure water (control) at 1.0 T with different concentrations; (b) linear correlation between r1 ($T1^{-1}$), r2 ($T2^{-1}$) and Gd concentration, based on reading from (a). The r1 and r2 relaxivities are the slope of the curve.

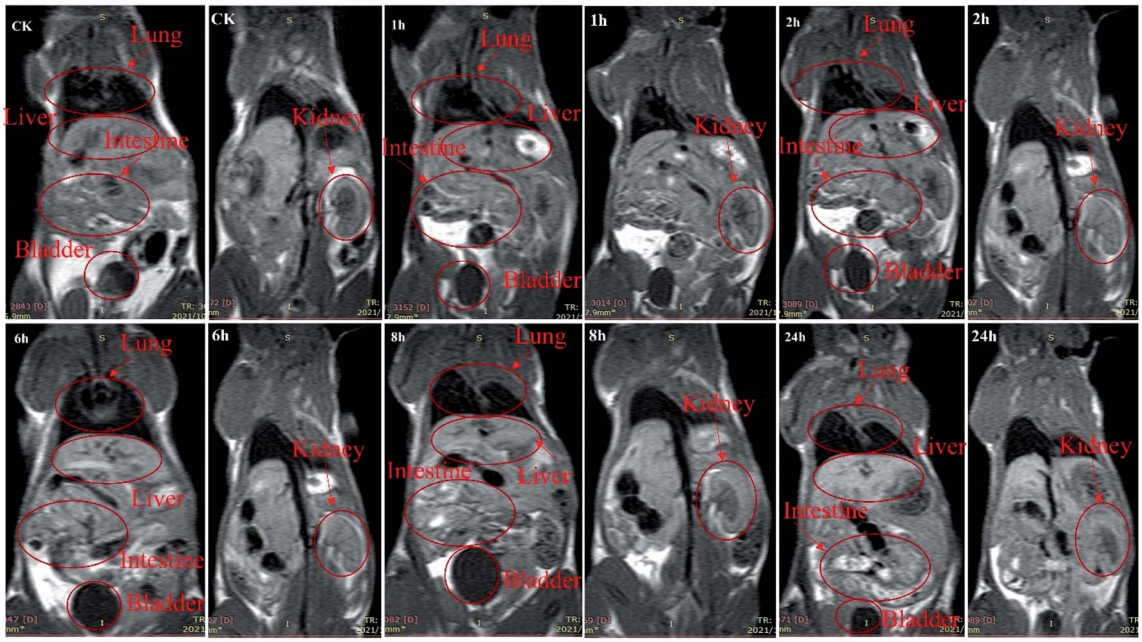

Fig. 4 *In vivo* MR imaging of PAL@Gd-0.5@PVA composite at pro-injection and post-injection 1, 2, 6, 8 and 24 h after tail vein injection.

PAL@Gd-0.5@PVA are 59.56 and 340.81 mM^{-1} S^{-1}, respectively. The value of r1 is approximately 15 times higher than the current clinical contrast agent (4.0 mM^{-1} S^{-1}),[29,30] and the ratio of r2/r1 is as low as 5.72, which is in the range of 0–10, indicating that the composite can be used as a T1 contrast agent.[31,32] The excellent contrast imaging performance may be attributed to the rod-like structure skeleton of PAL in the composite material, which is conducive to the easier access of water molecules in the environment to the Gd^{3+} loaded on the surface. Moreover. The residence time of water molecules in the unique nanopores of PAL on Gd^{3+} is prolonged due to their being bound, thereby further improving the relaxation performance.

In vivo MRI

The MRI contrast performance of the composite material was further verified by *in vivo* imaging. The PAL-Gd-0.5@PVA is formulated into a Gd^{3+} solution with a concentration of 1.6 mg L^{-1}, and 300 μL is injected into the tail vein of mice. The crown T1-weighted imaging of the mice at pro- and post-injection time point is shown in Fig. 4. It can be seen that compared with the whole-body image of the mice pro-injection, the brightness of the liver of the mice increases significantly with time for the post-injection images. At post-injection 4 h, the brightness in liver gradually decreases. After that, the brightness of the image further gradually decreases with time, and after 24 h, it basically returned to the level of pro-injection. Interesting, in contrast to the image of the liver, which gradually weakens over time, the image of the intestine becomes brighter over time. Even at post-injection 24 h, there is still a brighter signal in the intestinal area. This indicates that the prepared composite is mainly metabolized by the liver, and then eliminated through the intestine. In addition, the MRI signal in the kidney is also merged in the Fig. 4. The changes in the kidney signal over time are basically in sync with the liver. However, the brightness of the image in the kidney is obviously not that of the liver, indicating that renal clearance may not be the main metabolic pathway of the composite contrast agent. The above results further indicate that the smart designed PAL composite can improve the brightness of the T1 image of the animal model, which is of great significance for improving the accuracy of diagnosis, suggests the composite as a T1 type contrast material shows a good application prospect.

Moreover, in the three important parameters influencing the performances of contrast agent relaxation, a large number research is carried out about increasing the hydration number q and prolonging the rotational correlation time τ_R. However, there are few studies on improving relaxation rate by extending residence time of water molecules on gadolinium ions τ_m. This is mainly due to the constraints of water molecules is difficult. In recent years, the rapidly developing porous materials have been applied in various fields. The composite contrast agent is prepared by combining porous materials with gadolinium ions, and the binding effect of pores and channels of porous materials on water molecules is used to prolong the residence time of water molecules on gadolinium ions, thus greatly improving the relaxation properties of contrast agents, providing a new method for the development of new contrast agents.

Conclusion

In summary, a composite contrast agent based on PAL and gadolinium ions is smart designed and prepared by taking advantage of the restraint effect of the unique pores and channels of natural clay PAL on water molecules and introducing paramagnetic Gd^{3+} to the outlet of the pores and

channels through simple coordination polymerization. Due to the loss of freedom of water molecules in the pores and channels, the residence time on Gd^{3+} is greatly prolonged, thus improving the relaxation properties of the composite. The rod-like structure of PAL in the composite remains intact and plays a key role in skeleton support and crosslinking of the composite. The results of activity research show that the composite contrast agent exhibit high stability, good blood compatibility, low cell toxicity. Moreover, the longitudinal and transverse relaxation rates showed boost increases and reaching 59.56 and 340.81 mM^{-1} S^{-1}, respectively. *In vivo* imaging also displays enhanced MRI effects. Therefore, it is expected to be widely used as a new type of T1 contrast agent.

Conflicts of interest

The authors declare no competing financial interest.

Acknowledgements

The authors acknowledge the support of Natural Science Foundation of Gansu Province (No: 20JR10RA511, 2019B-084).

References

1 Y. Cai, Y. Wang, T. Zhang and Y. Pan, *ACS Appl. Nano Mater.*, 2020, **3**, 8771–8783.
2 K. Xu, N. Xu, B. Zhang, W. Tang and A. Hu, *Dalton Trans.*, 2020, **49**, 8927–8932.
3 W. B. Xu, J. Zhang, M. Z. Zhao, Z. J. Yang, Q. F. Wu and F. Nian, *J. Biomed. Nanotechnol.*, 2021, **17**, 1635–1646.
4 B. Li, T. T. Gong, N. N. Xu, F. Z. Cui, B. Y. Yuan, H. Z. Sun, L. Wang and J. H. Liu, *Small*, 2020, **16**, 2003969.
5 A. Rodríguez-Galván, M. Rivera, P. García-López, L. A. Medina and V. A. Basiuk, *J. Cell. Mol. Med.*, 2020, **24**, 3779–3794.
6 D. Waddington, T. Boele, R. Maschmeyer, Z. Kuncic and M. Rosen, *Sci. Adv.*, 2020, **6**, eabb0998.
7 S. Rayamajhi, R. Marasini, T. Nguyen, B. L. Plattner, D. Biller and S. Aryal, *Biomater. Sci.*, 2020, **8**, 2887–2904.
8 Z. Wang, L. He, B. Liu, L. P. Zhou, L. X. Cai, S. J. Hu, X. Z. Li, T. F. Chen, X. P. Li and Q. F. Sun, *J. Am. Chem. Soc.*, 2020, **142**, 16409–16419.
9 O. U. Akakuru, M. Z. Iqbal, C. Liu, J. Xing, Z. N. Wei, Z. Q. Jiang, Q. L Fang, B. Yuan, E. L. Nosike, J. B. Xia, Y. H. Jin, J. J. Zheng and A. G. Wu, *J. Cell. Mol. Med.*, 2020, **18**, 100524.
10 V. C. Pierre, S. M. Harris and S. L. Pailloux, *Acc. Chem. Res.*, 2018, **51**, 342–351.
11 T. J. Clough, L. Jiang, K. L. Wong and N. J. Long, *Nat. Commun.*, 2019, **10**, 1–14.
12 A. L. Villaraza, A. Bumb and M. W. Brechbiel, *Chem. Rev.*, 2010, **110**, 2921.
13 K. H. Xu, M. W. Wang, W. J. Tang, Y. Ding and A. G. Hu, *Chem.–Asian J.*, 2020, **15**, 2475–2479.
14 S. W. Guo, X. M. Wang, Y. Dai, X. H. Dai and K. Luo, *Adv. Sci.*, 2020, **7**, 2000467.
15 S. M. Zhang, Y. M. Zheng, D. Y. Fu, W. Li, Y. Q. Wu, B. Li and L. X. Wu, *J. Mater. Chem. B*, 2017, **5**, 4035–4043.
16 M. Salarian, R. C. Turaga, S. H. Xue, M. Nezafati, K. Hekmatyar, J. J. Qiao, Y. W. Zhang, S. S. Tan, O. Y. Lbhagui, Y. Hai, J. B. Li, R. Mukkavilli, M. Sharma, P. Mittal, X. Y. Min, S. Keilholz, L. Q. Yu, G. S. Qin, A. B. Farris, Z. R. Liu and J. J. Yang, *Nat. Commun.*, 2019, **10**, 1–14.
17 W. B. Xu, H. T. Long, X. X. Xu, G. R. Fu, L. M. Pu and L. Ding, *New J. Chem.*, 2018, **42**, 19344–19348.
18 W. B. Xu, Z. Y. Lin, G. C. Li, H. T. Long, M. Y. Du, G. R. Fu and L. M. Pu, *RSC Adv.*, 2019, **9**, 37052–37056.
19 D. J. Huang, W. B. Wang, J. X. Xu and A. Q. Wang, *Chem. Eng. J.*, 2012, **210**, 166–172.
20 J. H. Wang, D. Zhang, S. C. Liu and C. Y. Wang, *Sci. Total Environ.*, 2020, **720**, 137391.
21 J. X. Xu, J. P. Zhang, Q. Wang and A. Q. Wang, *Appl. Clay Sci.*, 2011, **54**, 118–123.
22 Z. F. Zhang, W. B. Wang and A. Q. Wang, *Appl. Clay Sci.*, 2015, **107**, 230–237.
23 A. Chahi, S. Petit and A. Decarreau, *Clays Clay Miner.*, 2002, **50**, 306–313.
24 Z. F. Zhang, W. B. Wang, Y. R. Kang, Q. Wang and A. Q. Wang, *Powder Technol.*, 2018, **327**, 246–254.
25 D. A. McKeown, J. E. Post and E. S. Etz, *Clays Clay Miner.*, 2002, **50**, 667–680.
26 J. Qin, G. H. Liang, Y. Y. Feng, B. X. Feng, G. Wang, N. Wu, Y. X. Zhao and J. Wei, *Nanoscale*, 2020, **12**, 6096–6103.
27 P. Liu and T. M. Wang, *Ind. Eng. Chem. Res.*, 2007, **46**, 97–102.
28 J. Wei, G. Wang, F. Chen, M. Bai, Y. Liang, H. T. Wang, D. Y. Zhao and Y. X. Zhao, *Angew. Chem., Int. Ed.*, 2018, **130**, 9986–9991.
29 S. Sagbas, N. Aktas and N. Sahiner, *Appl. Surf. Sci.*, 2015, **354**, 306–313.
30 S. Wang, G. C. Yu, Z. T. Wang, O. Jacobson, L. S. Lin, W. J. Yang, H. Z. Deng, Z. M. He, Y. Liu, Z. Y. Chen and X. Y. Chen, *Angew. Chem., Int. Ed.*, 2019, **131**, 14900–14905.
31 J. Jin, Y. Gao, Y. Wu, S. Liu and J. Zheng, *Powder Technol.*, 2021, **377**, 212–221.
32 Y. Q. Yu, Y. F. Ji, J. H. Lu, X. M. Yin and Q. S. Zhou, *Chem. Eng. J.*, 2021, **406**, 126759.
33 P. Liu, H. Wang and C. Pan, *Appl. Clay Sci.*, 2018, **159**, 37–41.
34 W. B. Xu, B. Mu and A. Q. Wang, *Cellulose*, 2017, **24**, 5579–5592.
35 W. B. Xu, B. Mu and A. Q. Wang, *Electrochim. Acta*, 2017, **224**, 113–124.
36 R. Chen, X. B. Zhou, Y. Wu, Q. Y. Liu, Q. Liu, J. H. Huang and F. Y. Li, *Sens. Actuators, B*, 2021, **328**, 129050.
37 M. Horstmann, R. G. de Vega, D. P. Bishop, U. Karst, P. A. Doble and D. Clases, *J. Anal. At. Spectrom.*, 2021, **36**, 767–775.